J|A|C|S ARTICLES

Published on Web 01/15/2009

Catalytic Consequences of Spatial Constraints and Acid Site Location for Monomolecular Alkane Activation on Zeolites

Rajamani Gounder and Enrique Iglesia*

Department of Chemical Engineering, University of California at Berkeley, Berkeley, California 94720

Received October 22, 2008; E-mail: iglesia@berkeley.edu

Abstract: The location of Brønsted acid sites within zeolite channels strongly influences reactivity because of the extent to which spatial constraints determine the stability of reactants and of cationic transition states relevant to alkane activation catalysis. Turnover rates for monomolecular cracking and dehydrogenation of propane and n-butane differed among zeolites with varying channel structure (H-MFI, H-FER, H-MOR) and between OH groups within eight-membered ring (8-MR) side pockets and 12-MR main channels in H-MOR. Measured monomolecular alkane activation barriers depended on catalyst and reactant properties, such as deprotonation enthalpies and proton affinities, respectively, consistent with Born−Haber thermochemical cycles that define energy relations in acid catalysis. Monomolecular alkane cracking and dehydrogenation turnovers occurred with strong preference on acid sites contained within smaller 8-MR pockets in H-MOR, while rates on sites located within 12-MR channels were much lower and often undetectable. This strong specificity reflects transition states that are confined only partially within 8-MR pockets; as a result, entropic gains compensate for enthalpic penalties caused by their incomplete containment to give a lower free energy for transition states within small 8-MR side pockets. These effects of entropy are stronger for dehydrogenation, with a later and looser transition state, than for cracking in the case of both propane and n-butane; therefore, selectivity can be tuned by the selective positioning or titration of OH groups within specific environments, the number of which was assessed in H-MOR by rigorous deconvolution of their infrared spectra. Specifically, cracking-to-dehydrogenation ratios for propane and n-butane were much smaller and terminal-to-central C−C bond cleavage ratios for n-butane were much larger on 8-MR than on 12-MR acid sites as a result of partial confinement, a concept previously considered phenomenologically as pore mouth catalysis. These marked effects of spatial constraints and of entropic factors on acid site reactivity and selectivity, also inferred for MFI from titration of OH groups by Na^+, have not been previously proposed or recognized and appear to be unprecedented in hydrocarbon catalysis. These findings and their conceptual interpretations open opportunities for the design of microporous solids by the rational positioning of acid sites within specific channel locations and with predictable consequences for catalytic rates and selectivities.

1. Introduction

The design and selection of acidic zeolites for specific reactions requires that we consider the consequences of the number, structure, and acid strength of active sites, and of intrachannel environments, within which sites stabilize adsorbed intermediates and transition states relevant to chemical transformations. At an early and defining moment in catalysis by zeolites, cracking rates of n-hexane on H-MFI zeolites were reported to depend only on the number of acid sites,[1,2] irrespective of Al content and, by inference, of the distribution of Al among the 12 crystallographic T-sites in MFI. Quantum chemical descriptions, however, indicated that the location of the Al atoms in MFI influenced Brønsted acid strength and reactivity.[3] Later studies rigorously accounted for long-range electrostatic interactions and found that deprotonation enthalpies (DPE) were instead similar for all Al sites in MFI (1229−1240 kJ mol^{-1}).[4,5] Acid strength, reflected rigorously in these DPE values, strongly influences activation barriers for reactions involving cationic transition states that are stabilized by electrostatic interactions with framework oxygens, which also stabilize protons removed in deprotonation events.[6,7] In contrast, acid strength influences only weakly reactions requiring activated complexes with low charge, which are stabilized by covalent bonds with the zeolite framework.[6,7]

We have recently reported the remarkable enzyme-like specificity of eight-membered ring (8-MR) channels in MOR zeolites for CO insertion into methyl groups, an elementary step that involves cationic transition states.[8] In contrast, the exchange of CD_4 with OH, which proceeds via essentially uncharged covalent transition states, showed similar rates on Brønsted acid

(1) Olson, D. H.; Haag, W. O.; Lago, R. M. *J. Catal.* **1980**, *61*, 390.
(2) Haag, W. O.; Lago, R. M.; Weisz, P. B. *Nature* **1984**, *309*, 539.
(3) Kazansky, V. B. *Acc. Chem. Res.* **1991**, *24*, 379.
(4) Eichler, U.; Brändle, M.; Sauer, J. *J. Phys. Chem. B* **1997**, *101*, 10035.
(5) Sauer, J.; Sierka, M. *J. Comput. Chem.* **2000**, *21*, 1470.
(6) van Santen, R. A.; Kramer, G. J. *Chem. Rev.* **1995**, *95*, 637.
(7) Rigby, A. M.; Kramer, G. J.; van Santen, R. A. *J. Catal.* **1997**, *170*, 1.
(8) Bhan, A.; Allian, A. D.; Sunley, G. J.; Law, D. J.; Iglesia, E. *J. Am. Chem. Soc.* **2007**, *129*, 4919.

10.1021/ja808292c CCC: $40.75

Table 1. Elemental Composition and Site and Structure Characterization of Zeolite Samples

zeolite	source	Si/Al ratio[a]	Na/Al ratio[a]	Al_{EF}[b] (%)	L_1 IR band area[c]	L_2 IR band area[c]	$OH_{8\text{-}MR}$[d] (%)	$OH_{12\text{-}MR}$[d] (%)
H-FER	Zeolyst	10.3	0.002	15	2.1	2.9	-	-
H-MFI-1	Chevron	19	-	24	0.6	0.1	-	-
H-MFI-2	Zeolyst	16.5	0.004	12	0.9	0.5	-	-
$H_{85}Na_{15}$MFI-2	Zeolyst	16.1	0.15	12	-	-	-	-
H-MFI-3	Zeolyst	25	-	11	0.3	<0.1	-	-
H-MFI-4	Zeolyst	40	-	11	0.2	<0.1	-	-
H-MOR-T	Tosoh	8.9	0.001	19	5.0	8.6	78	22
H-MOR-S	Sud-Chemie	10.1	0.001	21	10.4	4.9	60	40
H-MOR-Z	Zeolyst	10.0	0.001	22	2.8	3.9	56	44
$H_{83}Na_{17}$MOR-Z	Zeolyst	10.0	0.17	22	-	-	36	64
$H_{73}Na_{27}$MOR-Z	Zeolyst	10.0	0.27	22	-	-	27	73
$H_{59}Na_{41}$MOR-Z	Zeolyst	10.0	0.41	22	-	-	20	80
$H_{45}Na_{55}$MOR-Z	Zeolyst	10.0	0.55	22	-	-	13	87

[a] Determined from elemental analysis (ICP-OES; Galbraith Laboratories). [b] Extra-framework Al content (Al_{EF}) determined from ^{27}Al MAS NMR spectra (details given in Section S.1 of the Supporting Information). [c] Areas of L_1 (2224 cm^{-1}) and L_2 (2196 cm^{-1}) infrared bands for CO adsorbed at 123 K on Lewis acid sites (details shown in Section S.2 of the Supporting Information). Areas ($\times 10^3$) are normalized to Si−O−Si overtone band areas (2100−1750 cm^{-1}). [d] Distribution of acid sites in MOR samples determined from infrared spectral band deconvolution.[8]

sites present within 8-MR and 12-MR environments in MOR zeolites.[9] Strong effects of the local environment around Brønsted acid sites are not evident in previous studies of hydrocarbon catalysis, for which some studies have claimed no effects of Al content and, by inference, of their location.[1,2] Any catalytic consequences of site location, however, are essential to choose and synthesize inorganic microporous structures with specific reactivity and selectivity.

Here, we report evidence for strong effects of local structure on the catalytic cracking and dehydrogenation of alkanes on acidic zeolites. These reactions can occur via bimolecular pathways involving carbenium ion chain cycles[10,11] or via monomolecular routes requiring pentacoordinated carbonium ions at the transition state. Monomolecular routes prevail at low alkane conversions and pressures[12,13] and form H_2, smaller alkanes, and the respective alkenes as primary products (propane;[14] n-butane[15,16]). Isotopic studies indicate that products of monomolecular pathways initiate bimolecular routes mediated by carbenium ions, which then propagate via hydride transfer.[17,18] Monomolecular alkane reactions are useful probes of the catalytic consequences of confinement in acid catalysis, because they form relatively unreactive primary products of cracking (e.g., CH_4 and C_2H_4 from C_3H_8) and dehydrogenation (e.g., C_3H_6 and H_2 from C_3H_8) events. Deviations from equimolar yields provide a rigorous experimental kinetic marker for bimolecular or secondary reactions.

We interpret measured rate parameters here using thermochemical cycles that rigorously define the contributions of enthalpy and entropy to chemical reactions catalyzed by Brønsted acids. This approach illustrates the essential role of spatial constraints in the stabilization of adsorbed reactants and of ion pairs relevant for the late transition states prevalent in monomolecular alkane reactions. Energy−entropy tradeoffs at the transition state, mediated by local spatial constraints, are essential contributors to the enzyme-like specificity of certain locations within microporous solids for alkane activation on Brønsted acid sites.

2. Methods

2.1. Catalyst Synthesis. MFI, FER, and MOR zeolite samples (Table 1) in their NH_4^+ form were treated in flowing dry air (2.5 $cm^3\ g^{-1}\ s^{-1}$, zero grade, Praxair) by increasing the temperature to 773 K (0.0167 K s^{-1}) and holding for 4 h to convert NH_4^+ to H^+. H-zeolites were pelleted, crushed, and sieved to retain 180−250 μm (60−80 mesh) aggregates. Zeolite samples (∼14 g) were exchanged with Na^+ cations to varying extents using 0.5 L aqueous solutions with different $NaNO_3$ (99%, EMD Chemicals, 0.014−2.44 M) concentrations at 353 K for 12 h. The exchanged zeolite samples were rinsed with 2 L of deionized water, isolated by filtration, and treated in flowing dry air as described above. Si, Al, Na, and trace metal contents (Table 1) were determined by inductively coupled plasma optical emission spectroscopy (ICP-OES; Galbraith Laboratories). The amounts of Al in framework and extra-framework locations (Table 1) were measured by ^{27}Al MAS NMR spectroscopy. Experimental methods and NMR spectra are shown in Section S.1 of the Supporting Information.

2.2. Infrared Assessment of the Number and Location of Intracrystalline Hydroxyl Groups and Lewis Acid Centers. Infrared spectra were collected using a Nicolet NEXUS 670 infrared spectrometer equipped with a Hg−Cd−Te (MCT) detector. Spectra were measured with 2 cm^{-1} resolution in the 4000−400 cm^{-1} range by averaging 64 scans. Self-supporting wafers (∼20−40 mg) were sealed within a quartz vacuum infrared cell equipped with NaCl windows. Samples were treated in flowing dry air (1.67 $cm^3\ s^{-1}$, zero grade, Praxair) by heating to 723 K (0.033 K s^{-1}), holding for 2 h, and then evacuating for at least 2 h at 723 K using a diffusion pump (<0.01 Pa dynamic vacuum; Edwards E02) before cooling to 303 K in vacuum and collecting spectra.

Strong (L_1) and weak (L_2) Lewis acid centers were measured from infrared spectra of CO adsorbed at 123 K,[19] and specifically from CO bands at 2224 and 2196 cm^{-1}, respectively.[20] A constant flow of liquid N_2 was used to cool zeolites to 123 K before dosing CO (UHP, Praxair) incrementally, without intervening evacuation; spectra were collected 120 s after each CO dose. Integrated L_1 and

(9) Bhan, A.; Iglesia, E. *Acc. Chem. Res.* **2008**, *41*, 559.
(10) Greensfelder, B. S.; Voge, H. H.; Good, G. M. *Ind. Eng. Chem.* **1949**, *41*, 2573.
(11) Thomas, C. L. *Ind. Eng. Chem.* **1949**, *41*, 2564.
(12) Haag, W. O.; Dessau, R. M. Proceedings - International Congress on Catalysis, 8th, Berlin, Verlag Chemie: Weinheim, 1984; Vol. 2, p 305.
(13) Kotrel, S.; Knözinger, H.; Gates, B. C. *Microporous Mesoporous Mater.* **2000**, *35*−*36*, 11.
(14) Kwak, B. S.; Sachtler, W. M. H.; Haag, W. O. *J. Catal.* **1994**, *149*, 465.
(15) Krannila, H.; Haag, W. O.; Gates, B. C. *J. Catal.* **1992**, *135*, 115.
(16) Lercher, J. A.; van Santen, R. A.; Vinek, H. *Catal. Lett.* **1994**, *27*, 91.
(17) Ivanova, I. I.; Pomakhina, E. B.; Rebrov, A. I.; Derouane, E. G. *Topics Catal.* **1998**, *6*, 49.
(18) Ivanova, I. I.; Rebrov, A. I.; Pomakhina, E. B.; Derouane, E. G. *J. Mol. Catal. A* **1999**, *141*, 107.
(19) Cheung, P.; Bhan, A.; Sunley, G. J.; Law, D. J.; Iglesia, E. *J. Catal.* **2007**, *245*, 110.
(20) Benco, L.; Bucko, T.; Hafner, J.; Toulhoat, H. *J. Phys. Chem. B* **2004**, *108*, 13656.

Table 2. Monomolecular Propane Cracking and Dehydrogenation Rate Constants (k_{meas}) and Cracking-to-Dehydrogenation (C/D) Rate Ratios at 748 K and Measured Activation Energies (E_{meas}) and Entropies (ΔS_{meas}) on Acidic Zeolites

	k_{meas} ($\times 10^3$ mol (mol H^+)$^{-1}$ s^{-1} bar^{-1})			E_{meas} (kJ mol^{-1})		ΔS_{meas} (J mol^{-1} K^{-1})	
zeolite	cracking	dehyd	C/D ratio	cracking[a]	dehyd[b]	cracking[c]	dehyd[d]
H-MFI	2.0	2.1	0.9	158	200	−99	−54
H-FER	6.2	3.2	2.0	157	195	−91	−57
H-MOR-T	2.0	3.0	0.7	160	189	−97	−71
H-MOR-S	1.3	1.9	0.7	167	192	−93	−66
H-MOR-Z	1.4	2.2	0.7	160	198	−99	−56

[a] Errors are ± 5 kJ mol^{-1}. [b] Errors are ± 7 kJ mol^{-1}. [c] Errors are ± 8 J mol^{-1} K^{-1}. [d] Errors are ± 10 J mol^{-1} K^{-1}.

L_2 band areas (normalized to those for Si−O−Si overtones; 2100−1750 cm^{-1}) are proportional to the density of Lewis centers (per gram) in the sample and are shown in Table 1. The characterization of Lewis acid centers by these infrared methods is treated in more detail in Section S.2 of the Supporting Information.

2.3. Catalytic Rates of Monomolecular Alkane Activation. Steady-state alkane cracking and dehydrogenation rates were measured in a tubular packed-bed quartz reactor (7.0 mm inner diameter) with plug-flow hydrodynamics under differential conditions (<2% conversion). Catalyst samples (0.02−0.2 g) were supported on a coarse quartz frit, and the temperature was maintained with a resistively heated three-zone furnace (Applied Test Systems Series 3210). Each zone was controlled independently by Watlow controllers (96 Series); catalyst temperatures were recorded using K-type thermocouples contained within a thermowell placed at the external surface of the quartz reactor.

Catalysts were treated in a mixture of 5% O_2 in He (16.7 cm^3 g^{-1} s^{-1}, 99.999%, Praxair) at 803 K (0.0167 K s^{-1}) for 2 h before catalytic measurements. The samples were then treated in He (16.7 cm^3 g^{-1} s^{-1}, 99.999%, Praxair) for 0.5 h, while propane (10% C_3H_8, 99.999%, diluted in 5% Ar, 85% He, Praxair) or n-butane (10% n-C_4H_{10}, 99.99%, diluted in 5% Ar, 85% He, Praxair) reactants were sent via heated transfer lines held at 423 K to a gas chromatograph (Agilent HP-6890GC) for calibration purposes. Reactants and products were separated using GS-AL\KCl capillary (0.530 mm ID × 50 m; Agilent) and HayeSep DB packed columns (100−120 mesh, 10 ft.; Sigma-Aldrich); their respective effluents were measured by flame ionization and thermal conductivity detection.

Reactant pressures were changed by dilution with He (99.999%, Praxair). Reactant flows were varied (10^{-6}−10^{-4} mol alkane g^{-1} s^{-1}) to probe primary and secondary pathways and any contributions from bimolecular or secondary reactions. The absence of bimolecular pathways and secondary reactions was confirmed by the equimolar ratios of cracking products (1.0 ± 0.1) measured for C_3H_8 (C_2H_4/CH_4) and n-C_4H_{10} (C_3H_6/CH_4, C_2H_4/C_2H_6) reactants, which did not depend on space velocity, and by the absence of hydrocarbons larger than the respective alkane reactants. Activation energies and pre-exponential factors were obtained from rate constants measured as a function of temperature (718−778 K). Rates and selectivities measured after ∼100 ks on stream were similar (within 5%) to those at the start of each experiment on all catalyst samples. Transport corruptions of measured rates were ruled out using Mears criteria; the detailed analysis is shown in Section S.3 of the Supporting Information.

3. Results and Discussion

3.1. Assessment of Kinetic Parameters for Monomolecular Propane Cracking and Dehydrogenation Using Transition State Theory and Thermochemical Cycles. Table 2 shows rate constants (per H^+) for propane cracking and dehydrogenation and cracking-to-dehydrogenation rate ratios at 748 K on H-MFI, H-FER, and H-MOR, together with activation energies and entropies calculated from the temperature dependence of these rate constants. Monomolecular rate constants differ among these zeolites (by up to factors of 4) and even among H-MOR samples with similar Si/Al ratios but of different provenance (by up to factors of 2). Measured activation energies for dehydrogenation were consistently higher than for cracking (by 25−42 kJ mol^{-1}) on all samples, in contrast with activation energies for C_3H_8 dehydrogenation on H-MFI that vary widely among previous reports.[21−26] Measured activation entropies were also higher for dehydrogenation than for cracking, consistent with later transition states for dehydrogenation, in which the H−H bond is nearly formed at the transition state.[27] Rate parameters differ among these zeolites because their transition states differ in their energy and entropy relative to the gas-phase alkanes, as we discuss later in the context of the relevant thermochemical cycles; as a result, these rate parameters probe specific and subtle effects of local environment on the structure and energy of these transition states.

Accepted pathways for monomolecular reactions of alkanes (B) on intrazeolite Brønsted acids (H^+Z^-) are depicted schematically in Scheme 1a. Alkanes adsorb from the extracrystalline phase (B(g)) onto a Brønsted acid site within zeolite channels (B(z)) in quasi-equilibrated and essentially nonactivated steps. Transition state formalisms require that monomolecular rearrangements of adsorbed alkanes on Brønsted acid sites depend rigorously on the thermodynamic activity of reactants.[28] These treatments, shown in greater detail in Section S.4 of the Supporting Information, give a rate expression of the form:

$$r = \frac{k_B T}{h} \exp\left(\frac{-\Delta G^{o\dagger}}{R_g T}\right) \times \frac{\gamma_{H^+Z} C_{H^+Z} \gamma_{B_z} C_{B_z}}{\gamma_\dagger} \qquad (1)$$

Monomolecular alkane activation pathways require high temperatures, which favor low intrazeolite concentrations (C_{Bz}) and H^+ sites that remain essentially unoccupied during catalysis (evidence in Section S.3 of the Supporting Information). Calorimetric, gravimetric, and infrared studies on various acidic zeolites have shown that C_3−C_6 n-alkanes adsorb specifically onto Brønsted acid sites with adsorption enthalpies that remain constant up to saturation coverages at all H^+ sites.[29−31] Thus,

(21) Narbeshuber, T. F.; Vinek, H.; Lercher, J. A. *J. Catal.* **1995**, *157*, 388.
(22) Narbeshuber, T. F.; Brait, A.; Seshan, K.; Lercher, J. A. *J. Catal.* **1997**, *172*, 127.
(23) Wang, X.; Carabineiro, H.; Lemos, F.; Lemos, M. A. N. D. A.; Ribiero, F. R. *J. Mol. Catal. A* **2004**, *216*, 131.
(24) Bandiera, J.; Dufaux, M.; Ben Taarit, Y. *Appl. Catal., A* **1997**, *148*, 283.
(25) Bandiera, J.; Ben Taarit, Y. *Appl. Catal.* **1990**, *62*, 309.
(26) Xu, B.; Sievers, C.; Hong, S. B.; Prins, R.; van Bokhoven, J. A. *J. Catal.* **2006**, *244*, 163.
(27) Zheng, X.; Blowers, P. *J. Phys. Chem. A* **2005**, *109*, 10734.
(28) Madon, R. J.; Iglesia, E. *J. Mol. Catal. A Chem.* **2000**, *163*, 189.
(29) Eder, F.; Stockenhuber, M.; Lercher, J. A. *J. Phys. Chem. B* **1997**, *101*, 5414.
(30) Eder, F.; Lercher, J. A. *J. Phys. Chem. B* **1997**, *101*, 1273.
(31) Eder, F.; Lercher, J. A. *Zeolites* **1997**, *18*, 75.

Scheme 1. (a) Reaction Sequence for Monomolecular Alkane Activation on Brønsted Acid Sites Located within Zeolite Channels (H^+Z^-).[a] (b) Thermochemical Cycle for Monomolecular Reactions of Alkanes in Zeolite Channels[b]

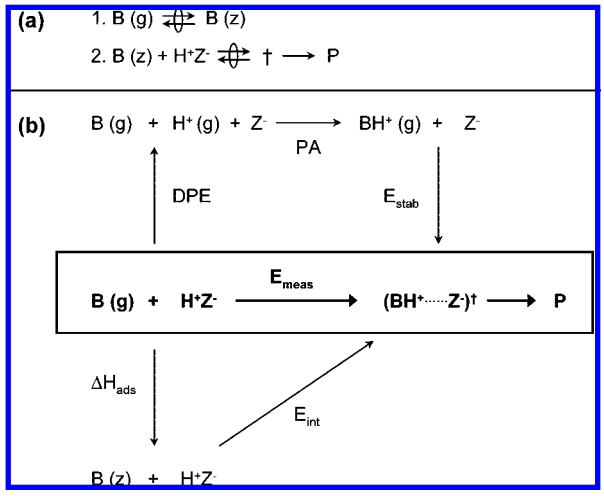

[a] B denotes a reactant base; P denotes products. [b] Measured activation energies (E_{meas}) are related to zeolite deprotonation enthalpies (DPE), gas-phase proton affinities (PA) and ion-pair stabilization energies within zeolite channels (E_{stab}). The dependence of intrinsic activation energies (E_{int}) on adsorption enthalpies (ΔH_{ads}) and E_{meas} (eq 6) is also shown.

Langmuir adsorption models accurately describe the siting of alkanes onto Brønsted acid sites of uniform binding properties. The concentrations (per active site) (C_i) of adsorbed alkanes (B_z) and transition states (†) are related to their real (P_B) or hypothetical ($P_\dagger$) gas-phase pressures by:

$$C_i = \frac{K_i P_i}{1 + K_B P_B + K_\dagger P_\dagger} \quad (2)$$

in which the K_i terms are their adsorption constants. Thermodynamic treatments of Langmuir surfaces give activity coefficients (γ_i) for each species of the form (derived in detail in Section S.4 of the Supporting Information):

$$\gamma_i = a_i^\circ(1 + K_B P_B + K_\dagger P_\dagger) \quad (3)$$

where a_i° is the thermodynamic activity at the reference state; activity coefficients (eq 3) include a configurational entropy term that reflects the number of configurations of N molecules adsorbed onto M adsorption sites.[32] Reaction rates are strictly proportional to intrazeolite alkane concentrations (C_{Bz}) when activity coefficients for alkane reactants (γ_{Bz}) and transition states ($\gamma_\dagger$) cancel in eq 1; this occurs in this case, irrespective of their structure and solvation, because both species reside on the same site and therefore have identical activity coefficients. Moreover, C_{H^+Z} and γ_{H^+Z} approach unity because H^+ sites are predominantly unoccupied during monomolecular reactions, for which the rates given by eq 1 become:

$$r = \frac{k_B T}{h} \exp\left(\frac{\Delta S^{\circ\dagger}}{R_g}\right) \times \exp\left(\frac{-\Delta H^{\circ\dagger}}{R_g T}\right) C_{Bz} \quad (4)$$

Intrazeolite concentrations (C_{Bz}) become proportional to external pressures (P_B) and to the adsorption constants (K_B) in the low-coverage limit (eq 2), where reaction rates (eq 4) are given by:

$$r = k_{int} K_B P_B \quad (5)$$

Measured activation energies and pre-exponential factors are then given by:

$$E_{meas} = E_{int} + \Delta H_{ads} \quad (6)$$

$$\ln(A_{meas}) = \ln(A_{int}) + (\Delta S_{ads}/R) \quad (7)$$

$$\Delta S_{meas} = \Delta S_{int} + \Delta S_{ads} \quad (8)$$

where ΔH_{ads} and ΔS_{ads} are the enthalpy and entropy of adsorption, respectively, and E_{meas} and A_{meas} (ΔS_{meas}) are measured rate parameters referenced to gas phase alkanes. E_{int} and A_{int} (ΔS_{int}) are intrinsic rate parameters for elementary reactions of adsorbed alkanes relating the properties of adsorbed reactants to the corresponding transition states.[21,33−36] We define the measured entropy of activation as:

$$\Delta S_{meas} = R[\ln(A_{meas}) - \ln(k_B T/h)] \quad (9)$$

where A_{meas} is rigorously normalized by the number of acid sites and by the number of bonds available for each type of reaction. These measured activation entropies reflect a mathematical manipulation that simply redacts A_{meas} in terms of thermodynamic properties of reactants and transition states.

Table 3 shows intrinsic activation energies and entropies for monomolecular propane cracking and dehydrogenation on H-MFI, H-FER, and H-MOR; these values were estimated from measured rate constants (Table 2), using eqs 6−9 and previously reported adsorption enthalpies and entropies.[29,30] Intrinsic activation barriers for monomolecular C_3H_8 cracking were similar on H-MFI, H-FER, and H-MOR (201−208 kJ mol^{-1}; Table 3), in agreement with previous data for C_3H_8 cracking on H-MFI (187−200 kJ mol^{-1}).[21−26] Their magnitude and insensitivity to zeolite structure also agree with previous reports for C_3H_8 cracking on H-MFI, H-MOR, H-BEA, and H-FAU[26] and for the cracking of larger C_3−C_{20} n-alkanes on H-MFI.[21,33,37] Energies of monomolecular cracking transition states (reflected in E_{meas}) relative to those of adsorbed reactants are independent of chain size and of local channel environments, which appear to stabilize adsorbed reactants and transition states identically. As a result, intrinsic activation barriers (E_{int}) for cracking reactions on different zeolite structures are similar within the accuracy of the rate and adsorption data used to estimate them (Table 3), as long as adsorption and rate measurements probe the same intrachannel environment.

Intrinsic activation energies for monomolecular propane dehydrogenation were also similar on H-MFI, H-FER, and H-MOR (229−245 kJ mol^{-1}; Table 3) and larger than for cracking (by 25−42 kJ mol^{-1}). These data contrast previous reports of intrinsic dehydrogenation barriers that varied widely for C_3H_8 among various H-MFI studies (135−205 kJ mol^{-1})[21−26] and which ranged from smaller barriers (by 60 kJ mol^{-1})[21−23] than for cracking to similar values[24,25] or even slightly larger values[26] than cracking barriers. Density functional theory (DFT) studies on small T3 zeolite clusters[27] concluded that transition states are ~60 kJ mol^{-1} higher in energy for dehydrogenation than cracking of propane. Figure 1 compares the temperature dependence of propane cracking-to-dehydrogenation rate ratios on H-MFI with DFT estimates[27] and previous data.[21,24,26] Only activation barriers were reported in DFT studies,[27] so we have

(32) Denbigh, K. *The Principles of Chemical Equilibrium*, 4th ed.; Cambridge University Press: Cambridge, 1981.
(33) Haag, W. O. *Stud. Surf. Sci. Catal.* **1994**, *84*, 1375.
(34) van Bokhoven, J. A.; Williams, B. A.; Ji, W.; Koningsberger, D. C.; Kung, H. H.; Miller, J. T. *J. Catal.* **2004**, *224*, 50.
(35) Babitz, S. M.; Williams, B. A.; Miller, J. T.; Snurr, R. Q.; Haag, W. O.; Kung, H. *Appl. Catal. A Gen.* **1999**, *179*, 71.
(36) Bhan, A.; Gounder, R.; Macht, J.; Iglesia, E. *J. Catal.* **2008**, *253*, 221.
(37) Wei, J. *Chem. Eng. Sci.* **1996**, *51*, 2995.

Table 3. Intrinsic Activation Energies (E_{int}) and Entropies (ΔS_{int}) for Monomolecular Propane Cracking and Dehydrogenation on Acidic Zeolites

			E_{int} (kJ mol^{-1})		ΔS_{int} (J mol^{-1} K^{-1})	
zeolite	ΔH_{ads} (kJ mol^{-1})	ΔS_{ads} (J mol^{-1} K^{-1})	cracking[a]	dehyd[b]	cracking[c]	dehyd[d]
H-MFI	−45[e]	−102[e]	204	245	3	47
H-FER	−49[f]	−109[f]	205	244	17	51
H-MOR-T	−41[g]	−85[g]	202	229	−12	13
H-MOR-S	−41[g]	−85[g]	208	234	−8	18
H-MOR-Z	−41[g]	−85[g]	201	239	−14	28

[a] Errors are ± 7 kJ mol^{-1}. [b] Errors are ± 9 kJ mol^{-1}. [c] Errors are ± 10 J mol^{-1} K^{-1}. [d] Errors are ± 13 J mol^{-1} K^{-1}. [e] Adsorption data reported in ref 29. [f] Adsorption data reported in ref 30. [g] Adsorption data reported *only* for 12-MR channels of H-MOR in ref 29.

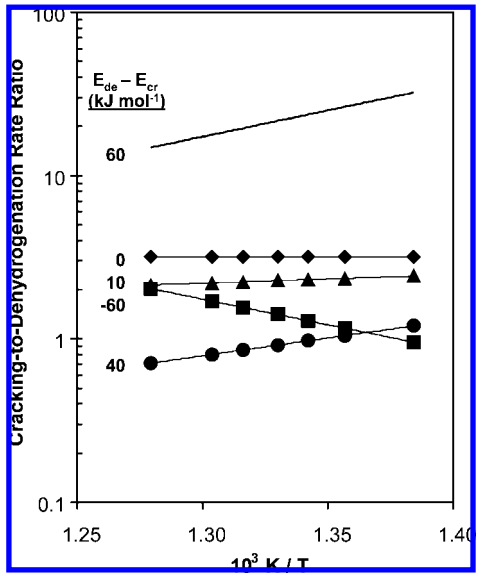

Figure 1. Temperature dependence of monomolecular propane cracking-to-dehydrogenation rate ratios on H-MFI. Differences in dehydrogenation (E_{de}) and cracking (E_{cr}) activation energies are reflected in the slope. Symbols denote experimentally measured rate ratios in this study (●) and rate ratios extrapolated from data reported in previous experimental studies (ref 21: ■, ref 24: ♦, ref 26: ▲) and in a theoretical study (ref 27: —).

used the pre-exponential factors (shown as ΔS_{meas} in Table 2) measured in this study to estimate cracking-to-dehydrogenation rate ratios from DFT activation barriers. All previous data show weaker temperature effects on rate ratios than reported here and predicted by theory (Figure 1). As we discuss below, higher barriers for dehydrogenation relative to cracking are also expected from the relative stabilities of protonated C−H and C−C bonds in C_3H_8 to form gas-phase structures resembling those in the respective transition states for these two reactions.

We use Born−Haber thermochemical cycles (Scheme 1b) to interpret the stabilization of reactants and transition states in acid catalysis by zeolites[38,39] and the contributions of intrachannel environments and transition state structure and charge to activation barriers. Measured activation energies (E_{meas}) reflect the stability of carbonium ion-like transition states stabilized within channels relative to gaseous reactants (B(g)). These barriers depend on the deprotonation enthalpies (DPE) of Brønsted acid sites, on proton affinities (PA) of gaseous reactants, and on transition state stabilization energies (E_{stab}) (Scheme 1b). The relations between measured activation energies (E_{meas}), reactant adsorption enthalpies (ΔH_{ads}), and intrinsic activation barriers (E_{int}) described by eq 6 are also depicted in Scheme 1b. In the context of this thermochemical cycle formalism, the following expressions relate measured and intrinsic activation barriers to properties of the acid, the molecules, and their ion pair at the transition state:

$$E_{meas} = DPE + PA + E_{stab} \quad (10)$$

$$E_{int} = DPE + PA + E_{stab} - \Delta H_{ads} \quad (11)$$

Deprotonation requires electron transfer from H atoms to the zeolite lattice (Z), cleavage of H−Z bonds, and separation of the H^+ and Z^- fragments to noninteracting distances. DPE values thus reflect contributions from homolytic H−Z bond dissociation energies (BDE), the ionization energy (IE) of H atoms, electron affinities (EA) of lattice oxygen atoms, and electrostatic interactions that stabilize the ion pair (H^+-Z^-) as separation proceeds. Any variation in DPE values among zeolite structures reflects predominantly the effects of the local environment on the electrostatic stabilization of the ion pair, because BDE, IE, and EA values are likely to depend weakly on spatial constraints. Hybrid quantum mechanical and interatomic potential methods indicate that DPE values for Brønsted acid sites at different T-sites in H-MFI (1229−1240 kJ mol^{-1})[4] and for the most stable Al location among H-MFI, H-FER, H-MOR zeolites (1218−1235 kJ mol^{-1})[5,40] are in fact similar. These similar deprotonation enthalpies reflect the predominant contributions from long-range interactions with the zeolite lattice to the electrostatic stabilization of protons, which overwhelm other contributions resulting from subtle variations in channel geometry.

Proton affinities reflect the energy required to protonate neutral gas-phase molecules (B) to form BH^+ complexes, which differ for cracking and dehydrogenation events because the C−C−H and C−H−H three-center/two-electron complexes formed by protonation of C−C and C−H bonds in alkanes differ in energy. Theoretical estimates[41,42] of gas-phase carbonium ion energies indicate that protonation of C−H bonds in C_3H_8 forms C−H−H three-center/two-electron species that are less stable by ∼20−40 kJ mol^{-1} than the C−C−H analogues formed via protonation of C−C bonds in C_3H_8.

Transition state energies reflect both electrostatic stabilization of ion pairs that form as BH^+ and Z^- interact and van der Waals stabilization of the organic cation in the transition state complex. Alkane adsorption enthalpies reflect predominantly van der Waals stabilization by framework oxygens and, to a lesser extent, any induced dipole interactions with H^+, where the latter do not depend on the size of alkane reactants or zeolite

(38) Aronson, M. T.; Gorte, R. J.; Farneth, W. E. *J. Catal.* **1986**, *98*, 434.
(39) Macht, J.; Janik, M. J.; Neurock, M.; Iglesia, E. *J. Am. Chem. Soc.* **2008**, *130*, 10369.
(40) Nieminen, V.; Sierka, M.; Murzin, D. Y.; Sauer, J. *J. Catal.* **2005**, *231*, 393.
(41) Esteves, P. M.; Mota, C. J. A.; Ramírez-Solís, A.; Hernández-Lamoneda, R. *J. Am. Chem. Soc.* **1998**, *120*, 3213.
(42) Collins, S. J.; O'Malley, P. J. *Chem. Phys. Lett.* **1994**, *228*, 246.

channels.[29−31] The positive charge (+0.9e) at the alkyl fragment in late monomolecular transition states is stabilized by long-range electrostatic interactions with the zeolite framework,[6,7,43,44] rendering subtle effects of channel size inconsequential for E_{stab}, the term that accounts for electrostatic stabilization in thermochemical cycles; similar long-range electrostatic considerations account for the weak dependence of DPE values on Brønsted acid site location or zeolite environment.[4,5,40] In contrast, van der Waals stabilization of adsorbed alkanes depends strongly on channel size and structure;[45] by inference, such stabilization is essential also for monomolecular transition states that resemble in structure their adsorbed alkane precursors. As a result, we conclude that differences in transition state stability (E_{stab}) among zeolite locations or structures are almost entirely compensated by commensurate differences in reactant stability (ΔH_{ads}), as evidenced by intrinsic activation barriers (E_{int}) that do not change with variations in the size or structure of zeolite channels (Table 3) or n-alkane reactants.[21,33,37]

The intrinsic activation barriers for alkane cracking and dehydrogenation on a given zeolite (or a given location within a zeolite) differ from each other primarily in the respective affinities for protonation of an alkane at C−C or C−H bonds, because DPE and ΔH_{ads} are independent of the specific reaction path for a given alkane and acid site (eq 11). The similar magnitude (+0.9e) and extent of charge delocalization in the organic fragment at cracking and dehydrogenation transition states[6,7,43,44] suggest that electrostatic stabilization (contained in E_{stab}) must also be insensitive to reaction path. The differences in intrinsic activation barriers for C_3H_8 dehydrogenation and cracking (estimated from rate data) for a given zeolite (25−42 kJ mol^{-1}; Table 3) must then reflect the calculated energy differences between three-center/two-electron C−H−H bonds (dehydrogenation) and C−C−H bonds (cracking) in the gas-phase (∼20−40 kJ mol^{-1}),[41,42] consistent with the thermochemical cycle in Scheme 1b and eq 11.

Thermochemical cycles that relate transition state energies to either gas-phase or adsorbed reactants (Scheme 1b) can also be used to describe the contributions of various catalyst and molecule properties to activation entropies. Measured activation entropies for cracking and dehydrogenation reflect differences in entropies between their respective transition states, because both are referenced to the same gas-phase reactant. Measured activation entropies for propane dehydrogenation are ∼40 J mol^{-1} K^{-1} larger than for cracking on H-MFI, H-FER, and H-MOR (Table 2), consistent with later transition states for dehydrogenation, in which H−H bonds are nearly formed (0.079 nm vs 0.074 nm in H_2(g)).[27] The late transition states prevalent in monomolecular alkane reactions[27,43,44] lead to hindered rotations and rocking vibrations[46] that increase entropy upon formation of the transition state from adsorbed reactants. As a result, intrinsic rate constants for monomolecular n-hexane cracking are ∼50 times larger than for propane cracking on H-MFI,[37] even though both reactions show similar intrinsic activation barriers. We *surmise* that such late transition states for dehydrogenation allow greater rotational and vibrational freedom for C_3H_7 and H_2 fragments than for the corresponding C_2H_5 and CH_4 groups at the earlier transition states involved in cracking reactions.

Scheme 2. Relations between Measured Activation Energies (E_{meas}), Adsorption Enthalpies (ΔH_{ads}), and Intrinsic Activation Energies (E_{int}) Are Shown Schematically for Two Different Channel Environments[a]

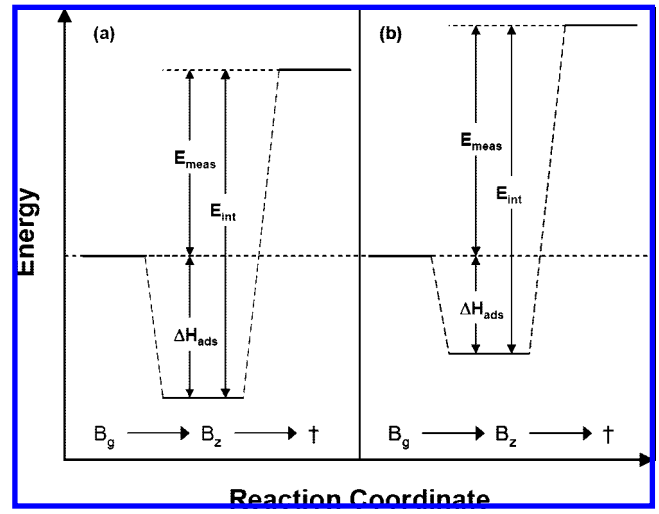

[a] Adsorbed reactants and transition states in location a are stabilized to a greater extent than in location b.

Scheme 2 depicts a hypothetical reaction coordinate diagram for acid sites within two environments with different spatial constraints, as a result of differences in either the identity of the zeolites or the siting of the acid within a specific location in a given zeolite structure. The more constrained environment in Scheme 2a stabilizes both adsorbed molecules and transition states more effectively than the more open structure in Scheme 2b through concerted interactions that influence the adsorption enthalpies of the reactants and the stabilization energies of the transition states,[45,47] assuming their *complete containment* within the smaller environment. Thus, intrinsic activation barriers for cracking (or dehydrogenation) are more weakly affected by local environment than measured activation energies, which reflect differences between transition states and gas-phase reactants. Measured turnover rates therefore depend on transition state energies and entropies, which depend, in turn, on the channel environment that stabilizes transition states but not reactants in the gas phase external to the zeolite.

H-MOR contains Al atoms that reside at four unique T-sites and corresponding Brønsted acid sites that reside within two distinct channel environments: 8-MR side pockets or 12-MR main channels. The distribution of Brønsted acid sites among 8-MR and 12-MR locations can be measured from the frequency and intensity of their antisymmetric vibrations in infrared spectra (3550−3650 cm^{-1}).[8] Such methods are unable to establish the specific location of OH groups in H-MFI, however, because of the greater diversity of T-sites and because intrachannel environments are more uniform in local structure in MFI than in MOR.[48] All acid sites in H-MFI reside within 10-MR channels or their intersection, precluding the use of titrants of varying size to probe local environment. In light of these considerations, we choose to examine the catalytic consequences of Al siting in the bimodal distribution of channel environments

(43) Zygmunt, S. A.; Curtiss, L. A.; Zapol, P.; Iton, L. E. *J. Phys. Chem. B* **2004**, *104*, 1944.
(44) Frash, M. V.; van Santen, R. A. *Topics Catal.* **1999**, *9*, 191.
(45) Savitz, S.; Siperstein, F.; Gorte, R. J.; Myers, A. L. *J. Phys. Chem. B* **1998**, *102*, 6865.
(46) Benson, S. W. *Thermochemical Kinetics*; Wiley: New York, 1976.
(47) Hunger, B.; Heuchel, M.; Clark, L. A.; Snurr, R. Q. *J. Phys. Chem B* **2002**, *106*, 3882.
(48) Busca, G. *Chem. Rev.* **2007**, *107*, 5366.

Table 4. Monomolecular Propane Cracking and Dehydrogenation Rate Constants (k_{meas}) and Cracking-to-Dehydrogenation Rate Ratios Measured at 748 K and Measured Activation Energies (E_{meas}) and Entropies (ΔS_{meas}) on Partially Na^+ Exchanged MOR-Z Samples

	k_{meas} ($\times 10^3$ mol (mol H^+)$^{-1}$ s^{-1} bar^{-1})			E_{meas} (kJ mol^{-1})		ΔS_{meas} (J mol^{-1} K^{-1})	
zeolite	cracking	dehyd	C/D ratio	cracking[a]	dehyd[b]	cracking[c]	dehyd[d]
$H_{100}Na_0$MOR-Z	1.4	2.2	0.7	160	198	−99	−56
$H_{83}Na_{17}$MOR-Z	1.2	1.2	1.0	160	201	−101	−58
$H_{73}Na_{27}$MOR-Z	1.1	0.8	1.4	157	201	−105	−60
$H_{59}Na_{41}$MOR-Z	0.9	0.6	1.5	155	196	−110	−69
$H_{45}Na_{55}$MOR-Z	0.6	0.3	1.7	153	198	−115	−72

[a] Errors are ± 5 kJ mol^{-1}. [b] Errors are ± 7 kJ mol^{-1}. [c] Errors are ± 8 J mol^{-1} K^{-1}. [d] Errors are ± 10 J mol^{-1} K^{-1}.

of H-MOR. Al siting was previously shown to strongly influence the stability of charged transition states involved in CO insertion into methyl groups[8] but not symmetric and essentially neutral transition states involved in exchange reactions.[9]

3.2. Catalytic Consequences of 8-MR and 12-MR Environments within MOR in Monomolecular Cracking and Dehydrogenation of Propane. Monomolecular propane cracking and dehydrogenation turnover rates (per H^+) differ by factors of ~2 (Table 2) on H-MOR zeolites with similar Al content. This range of reactivity does not reflect differences in the number of extraframework Al species or Lewis acid centers among these samples, as shown by the NMR and IR data in Sections S.1 and S.2, respectively, of the Supporting Information. Table 4 shows propane cracking and dehydrogenation rate constants (per total H^+) and cracking-to-dehydrogenation rate ratios at 748 K on H-MOR samples partially exchanged with Na^+, together with measured activation energies and entropies. Cracking and dehydrogenation rate constants (per residual H^+) decreased, and their rate ratio increased as H^+ species within H-MOR were selectively replaced by Na^+. Measured activation entropies for both cracking and dehydrogenation (eq 9; from rate constants normalized by residual H^+ sites) decreased monotonically with the extent of Na^+ exchange, but measured activation energies remained essentially constant.

The number of OH groups within 8-MR and 12-MR environments in H-MOR was measured from the intensity of antisymmetric OH stretches (~3550−3650 cm^{-1}) using reported methods.[8] Singular value decomposition was used to extract principal component spectra for OH bands in 8-MR and 12-MR locations centered at 3592 cm^{-1} and 3611 cm^{-1}, respectively.[8] These values are similar to those reported earlier on H-MOR (8-MR: ~3590 cm^{-1}; 12-MR: ~3610 cm^{-1})[49−51] and to those for residual OH groups after selective titration of 12-MR sites by pyridine.[8,49,50] The contribution from each pure component band was determined by least-squares regression methods that allowed each pure component band center to shift up to 3 cm^{-1} and assumed similar molar extinction coefficients for OH groups in the two locations. The deconvoluted infrared spectra for H-MOR-T and H-MOR-S are shown in Figure 2 and elsewhere for partially Na^+-exchanged H-MOR-Z samples.[8] The number of OH groups within 8-MR and 12-MR locations is listed in Table 1 for all MOR samples used in this study.

Infrared spectra showed that Na^+ cations selectively replace protons within constrained 8-MR side pockets in MOR[8,49,52] (Figure 3), because more electropositive alkali cations appear

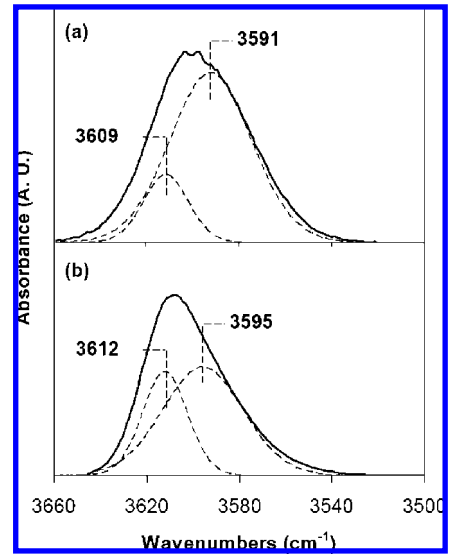

Figure 2. Infrared spectra (—) of (a) H-MOR-T (OH in 8-MR = 78 ± 5%) and (b) H-MOR-S (OH in 8-MR = 60 ± 5%). Deconvoluted bands (--) for 8-MR and 12-MR OH groups are shown along with their respective band centers.

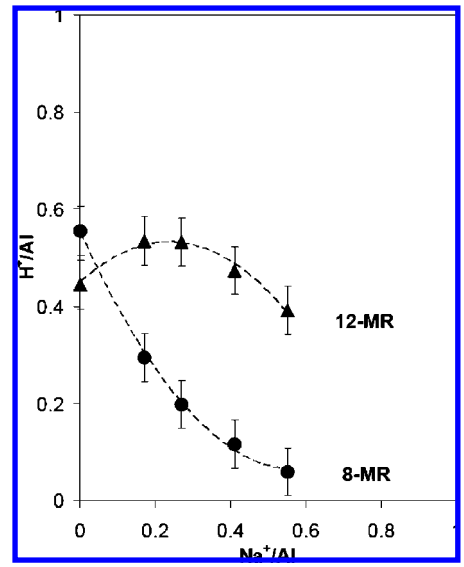

Figure 3. Number of residual protons (per Al) in 8-MR pockets (●) and 12-MR channels (▲) of MOR-Z samples with varying Na^+ content (per Al) determined by infrared spectral band deconvolution.[8]

to be stabilized more effectively than H^+ by the stronger dispersive forces prevalent within such smaller environments. Rate constants for C_3H_8 dehydrogenation (per residual H^+) decreased even more strongly with Na^+ exchange than for cracking (Table 4), reflecting a greater specificity of 8-MR

(49) Makarova, M. A.; Wilson, A. E.; van Liemt, B. J.; Mesters, C.; de Winter, A. W.; Williams, C. *J. Catal.* **1997**, *172*, 170.
(50) Datka, J.; Gil, B.; Kubacka, A. *Zeolites* **1997**, *18*, 245.
(51) Maache, M.; Janin, A.; Lavalley, J. C.; Benazzi, E. *Zeolites* **1995**, *15*, 507.
(52) Veefkind, V. A.; Smidt, M. L.; Lercher, J. A. *Appl. Catal., A* **2000**, *194*, 319.

Table 5. Monomolecular Propane Cracking and Dehydrogenation Rate Constants (k_{meas}) at 748 K within 8-MR and 12-MR Locations of MOR and Measured Activation Energies (E_{meas}) and Entropies (ΔS_{meas})[a]

reaction (location)	k_{meas}[b] ($\times 10^3$ mol (mol H^+)$^{-1}$ s^{-1} bar^{-1})	E_{meas} (kJ mol^{-1})	ΔS_{meas} (J mol^{-1} K^{-1})
cracking (8-MR)	2.0 ± 0.5	164 ± 5	-91 ± 9
cracking (12-MR)	0.7 ± 0.4	151 ± 5	-117 ± 14
dehydrogenation (8-MR)	3.2 ± 0.7	197 ± 7	-54 ± 11
dehydrogenation (12-MR)	n.d.[c]	n.d.[c]	n.d.[c]

[a] Uncertainties in regressed rate parameters are reported as twice the standard error. [b] Rate parameters determined by least-squares regression. [c] n.d., not detected.

pockets for dehydrogenation reactions compared with 12-MR channels. Measured activation entropies became more negative for both cracking and dehydrogenation as Na^+ replaced H^+ within 8-MR side pockets (Table 4), demonstrating that the more constrained environment provided by such pockets actually stabilizes looser transition states than the larger 12-MR main channels in MOR for both reactions.

We can extract from these data the specific contributions of OH groups within 8-MR and 12-MR locations in H-MOR by expressing measured rate constants for C_3H_8 cracking and dehydrogenation as linear combinations of rate constants in the two locations:

$$k = k_{8-MR}X_{8-MR} + k_{12-MR}X_{12-MR} \quad (12)$$

Here, $X_{8\text{-}MR}$ and $X_{12\text{-}MR}$ represent the fraction of all OH groups located within 8-MR and 12-MR locations, respectively, and $k_{8\text{-}MR}$ and $k_{12\text{-}MR}$ the corresponding monomolecular rate constants in each environment. The latter were determined by regressing overall rate constants on seven MOR samples with different acid site densities and location; the details of the regression analysis are shown in Section S.5 of the Supporting Information. Measured rate constants (shown at 748 K in Table 5) for C_3H_8 cracking were larger (by factors of ~3) in 8-MR than in 12-MR environments; C_3H_8 dehydrogenation rates on OH groups within 12-MR channels were undetectable within the accuracy of these measurements.

Brønsted acid sites within the more constrained 8-MR side pockets in H-MOR catalyze monomolecular cracking and dehydrogenation reactions of C_3H_8 preferentially (Table 5) over sites of similar acid strength[53] within the less constrained 12-MR channels. Propane dehydrogenation rates (per gram) are strictly proportional to the number of residual H^+ within 8-MR environments (per gram) and do not depend on the number of residual H^+ within 12-MR channels (per gram) (Figure 4), consistent with the exclusive reactivity of Brønsted acid sites of OH groups within 8-MR pockets at the conditions of these experiments (Table 5). Such remarkable specificity demonstrates the essential role of local environment on the enthalpic or entropic stabilization of dehydrogenation transition states. These data also illustrate how reactivity, as reflected here in turnover rates, varies significantly among the diverse T-site locations even within a given zeolite structure. These trends resemble those reported recently for CO insertion into adsorbed methyl groups derived from dimethyl ether, which formed acetyl groups (and ultimately methyl acetate after subsequent methoxylation with dimethyl ether) only on sites contained within 8-MR environments in H-MOR and H-FER.[8]

The systematic increase in cracking-to-dehydrogenation rate ratios (0.7 to 1.7; Table 4) as Na^+ replaced H^+ within 8-MR environments reflects the stronger effects of local environment on dehydrogenation transition states compared with cracking transition states. Propane cracking rates (per gram) were also proportional to the number of H^+ sites present within 8-MR environments (per gram), but detectable cracking contributions from OH groups in 12-MR channels cause a nonzero intercept (Figure 5). The rigorous subtraction of the 12-MR OH contributions (the second term in eq 12) from measured rates led to a strictly linear dependence of residual rates on the number of OH groups within 8-MR pockets and to a zero intercept, as shown by the dashed line in Figure 5.

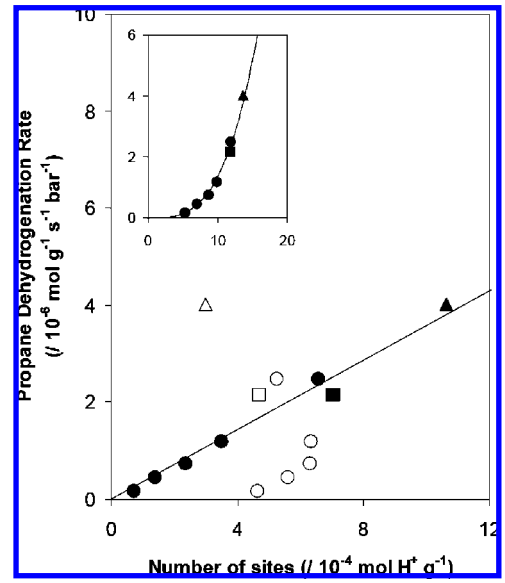

Figure 4. Propane dehydrogenation rates (per gram) at 748 K in H-MOR and Na^+-exchanged MOR samples (MOR-Z: ● MOR-S: ■, MOR-T: ▲) plotted against the density of Brønsted acid sites (per gram) in the 8-MR pockets of MOR (closed symbols) and 12-MR channels of MOR (open symbols). Inset shows propane dehydrogenation rates (per gram) plotted against the total density of Brønsted sites (per gram).

These data demonstrate that propane cracking and dehydrogenation occur preferentially within 8-MR pockets at 718−778 K on H-MOR. Yet, infrared bands of OH groups in 8-MR pockets of H-MOR were not perturbed by contact with C_3H_8 at near ambient temperatures (323 K),[29] suggesting that propane molecules have restricted access to or weaker interactions with 8-MR compared with 12-MR OH groups. ^{13}C NMR spectra[54] and theoretical simulations,[55] however, have shown that C_3H_8 adsorbs preferentially within 8-MR H-FER channels of similar size at ambient temperatures. Such specificity for adsorption within 12-MR channels in H-MOR reflects stronger dispersive forces within constrained environments that can *fully* contain the adsorbate molecules[45] and the consequently more negative

(53) Brändle, M.; Sauer, J. *J. Am. Chem. Soc.* **1998**, *120*, 1556.

(54) van Well, W. J. M.; Cottin, X.; de Haan, J. W.; Smit, B.; Nivarthy, G.; Lercher, J. A.; van Hooff, J. H. C.; van Santen, R. A. *J. Phys. Chem. B* **1998**, *102*, 3945.

(55) van Well, W. J. M.; Cottin, X.; Smit, B.; van Hooff, J. H. C.; van Santen, R. A. *J. Phys. Chem. B* **1998**, *102*, 3952.

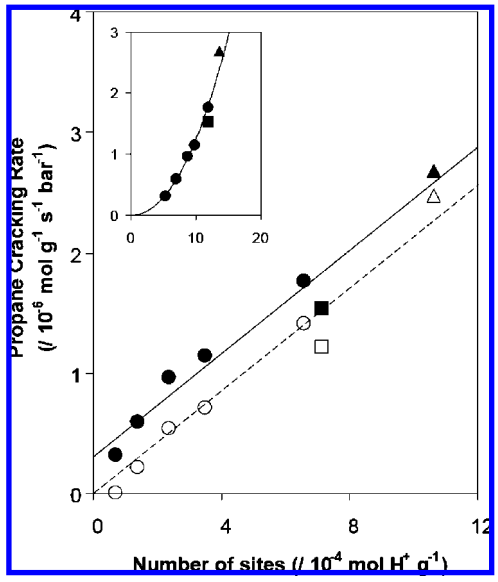

Figure 5. Measured propane cracking rates (per gram) (closed symbols) and residual cracking rates after correction for the contribution from 12-MR sites (per gram) (open symbols) at 748 K in H-MOR and Na^+-exchanged MOR samples (MOR-Z: ● MOR-S: ■, MOR-T: ▲) plotted against the density of Brønsted acid sites (per gram) in 8-MR pockets. Inset shows total propane cracking rates (per gram) plotted against the total density of Brønsted sites (per gram).

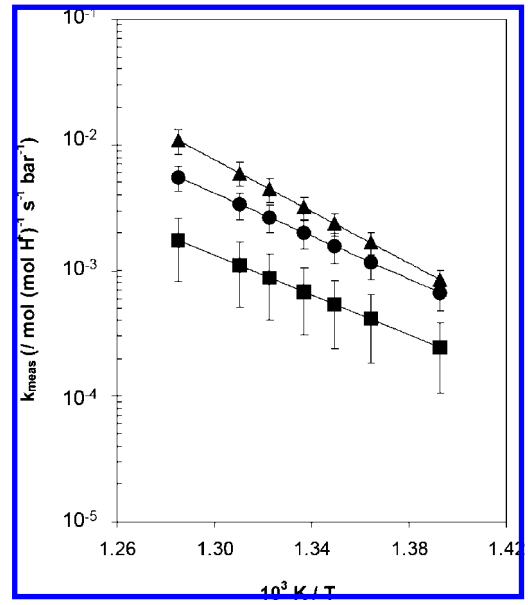

Figure 6. Measured rate constants (k_{meas}) for monomolecular propane cracking in 8-MR pockets (●) and 12-MR channels (■) and dehydrogenation in 8-MR pockets (▲) determined from least-squares regression analysis. Dehydrogenation rate constants were not detected in 12-MR channels. Error bars are shown as twice the standard error in regressed rate constants.

adsorption enthalpies that reflect more effective van der Waals contacts with framework oxygens.[29−31] Correlations that relate adsorption enthalpies to the effective channel diameters for different zeolites[45] predict that C_3H_8 would indeed adsorb more strongly (by ∼12 kJ mol^{-1}) *if fully contained* within channels 0.41 nm in diameter, such as those in 8-MR MOR pockets, than within the larger channels (0.67 nm) formed by 12-MR structures in MOR. C_3H_8 molecules (∼0.65 nm in length) extend, however, beyond the depth of the 8-MR pockets (∼0.37 nm) and must protrude into connecting 12-MR channels (procedures used for estimating channel and molecular dimensions are described in Sections S.6 and S.7, respectively, of the Supporting Information). These dimensions preclude van der Waals interactions between the entire propane molecule and the framework oxygens in 8-MR pockets. As a result, C_3H_8 adsorbs preferentially within larger 12-MR channels, which interact with the entire molecule, albeit more weakly than 8-MR channels able to contain the entire molecule.

Regressed rate constants on acid sites within 8-MR and 12-MR locations are shown as a function of temperature in Figure 6; these data were used to estimate activation energies and entropies within these two distinct MOR environments (Table 5). Cracking turnover rates were larger on sites present within 8-MR pockets than on acid sites of similar strength within 12-MR channels, even though measured activation energies were actually higher on 8-MR OH groups (by 13 kJ mol^{-1}), apparently because of looser transition states with higher entropies (Table 5). The adsorption enthalpy of C_3H_8 on 12-MR MOR channels was measured to be −41 kJ mol^{-1} using calorimetry,[29] in agreement with the adsorption enthalpy predicted from its correlation to channel size.[45] Taken together with the measured activation energy on 12-MR channels (151 kJ mol^{-1}), this enthalpy gives an intrinsic cracking activation barrier of 192 ± 7 kJ mol^{-1} for acid sites within 12-MR channels (eq 6). These data agree well with values for C_3H_8 cracking on H-MFI, H-FER and H-MOR (201−208 kJ mol^{-1}; Table 3). C_3H_8 adsorption enthalpies on 8-MR pockets are not available, but we can extend arguments and data indicating that intrinsic activation barriers are independent of zeolite structure or location (because they lead to equivalent stabilization of adsorbed precursors and transition states) to estimate such adsorption enthalpies from measured activation energies on 8-MR OH groups. Adsorption enthalpies for C_3H_8 within 8-MR H-MOR pockets would then be −30 kJ mol^{-1} in order for intrinsic cracking activation barriers to be the same as those determined on 12-MR H-MOR channels (∼190 kJ mol^{-1}). These data and arguments lead us to conclude that C_3H_8 adsorption is much weaker on 8-MR pockets in MOR than predicted based on channel size considerations (−53 kJ mol^{-1}; Section S.6 of the Supporting Information). Thus, we conclude that both adsorbed C_3H_8 molecules and their monomolecular transition states are only *partially* contained within shallow 8-MR pockets and protrude into neighboring 12-MR channels. These data and conclusions are consistent with measured transition state entropies (ΔS_{meas}), which are significantly higher on 8-MR than on 12-MR acid sites (Table 5).

We conclude that transition states are less stable, in terms of enthalpy, within 8-MR pockets, which can confine only in part cracking and dehydrogenation transition states, than within 12-MR channels, which provide more effective van der Waals stabilization for both the transition states and the adsorbed molecules. We note that partial containment destabilizes species by decreasing van der Waals contacts with parts of the molecules, but such contacts are not essential for electrostatic stabilization of the positive charge (+0.9e) at the three-atom/two-electron center in the transition state; in late transition states for monomolecular alkane reactions, the positive charge is localized at the carbon atom in the alkyl fragment left behind upon elimination of the neutral molecule (H_2 or CH_4) from the transition state. Turnover rates are higher for these partially confined species, in spite of the concomitant enthalpic destabilization caused by partial confinement, indicating that their free energies are in fact lower than for similar species fully

contained within 12-MR channels. These findings illustrate the dominant role of entropy in the stabilization of adsorbed species and transition states within confined environments and further extend our previous studies that concluded the exponential increase in monomolecular cracking rates of C_3-C_6 n-alkanes on H-MFI to reflect predominantly larger transition state entropies.[37]

The entropy component of transition state free energies, and, by extension, the benefits of the trade-offs mediated by partial containment, becomes increasingly significant for later transition states involving dissociation and elimination of a fragment from the activated complex, and causes atypically large pre-exponential factors ($10^{15}-10^{17}$ s^{-1}) for gas-phase fission reactions.[46] As a result, the specificity of 8-MR channels is even stronger for dehydrogenation than for cracking transition states, because of the later nature of the former,[27] as found experimentally (Table 5). We were unable to detect dehydrogenation contributions from 12-MR sites because of their low reactivity at the conditions of our measurements, precluding a similar analysis to that used above for 8-MR pockets to infer partial containment and enthalpy−entropy trade-offs in cracking transition state free energies. The similar nature of cracking and dehydrogenation transition states, however, leads us to conclude that similar effects of partial containment are responsible for the preferential stabilization of dehydrogenation transition states within 8-MR pockets in MOR.

The less negative transition state entropies (relative to reactants in the gas phase) measured for OH groups within 8-MR pockets (Table 5) reflect the strong effects of local environment on cracking and dehydrogenation rate constants and on cracking-to-dehydrogenation rate ratios and the concomitant changes in these properties among H-MOR samples with different OH distributions (Tables 2 and 4). The dependence of propane cracking-to-dehydrogenation rate ratios (at 748 K) on the fraction of all OH groups present within 8-MR H-MOR pockets is shown in Figure 7, together with values predicted from eq 12 and regressed rate constants (Table 5), which agree well with data on H-MOR samples of different provenance and for H-MOR samples in which Na^+ exchange was used to selectively titrate 8-MR OH groups.

We conclude that selectivity in alkane activation reactions can be tuned using the location of acid sites within a given zeolite structure. Temperature, which exploits differences in activation energies between dehydrogenation and cracking pathways, can also be used to control selectivity but relies solely on intrinsic differences in relative stabilities of reactants protonated at various positions or bonds; these relative intrinsic barriers for cracking and dehydrogenation are therefore independent of zeolite structures or channel location (Table 3), as predicted by the thermochemical cycle in Scheme 1b. Our findings provide an alternate strategy for selectivity control, which exploits location-specific differences in entropy between dehydrogenation and cracking transition states. To our knowledge, the ability to exploit location and zeolite structure to tune the selectivity of cracking and dehydrogenation pathways and the interpretation of the resulting effects in terms of the dominant effects of transition state entropies have not been previously recognized in zeolite catalysis. These data and conclusions provide design strategies for the placement of Al sites within specific locations in order to promote specific reactions via rigorous considerations of the position of their respective transition states along the reaction coordinate.

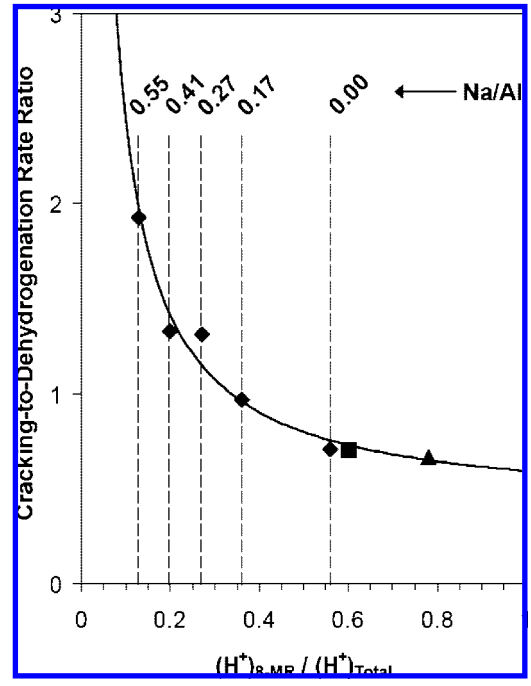

Figure 7. The dependence of propane cracking-to-dehydrogenation rate ratios at 748 K on the fraction of Brønsted acid sites in 8-MR pockets of MOR, predicted using regressed rate constants (Table 5) and eq 12, is given by the solid curve. Data at 748 K are shown (MOR-Z: ● MOR-S: ■, MOR-T: ▲) along with Na/Al ratios for MOR-Z samples.

To our knowledge, the enzyme-like specificity of spatial environments within 8-MR pockets in H-MOR or the marked effects of partial confinement have not been previously recognized or demonstrated for alkane activation reactions. These findings resemble, however, the reported specificity of 8-MR pockets for CO insertion into CH_3 groups during dimethyl ether carbonylation to methyl acetate at ~450 K[8]. The sole mechanistic connection between these reactions and the alkane activation reactions that we discuss here is the common involvement of cationic transition states. Such specificity was not observed for isotopic exchange reactions on zeolites, for which transition states are symmetrical and essentially uncharged.[9] We conclude that this remarkable specificity and the partial confinement effects responsible for it are general features of chemical reactions occurring via transition states with highly localized cationic centers within constrained environments. We provide next evidence for the role of partial confinement on the relative reactivity of various C−C bonds within alkanes in monomolecular cracking reactions and demonstrate the ability of H-MOR side pockets to selectively crack terminal C−C bonds in n-butane as a result of partial confinement configurations.

3.3. Partial Confinement Effects and Preferential Terminal Cracking Selectivity in n-Butane Activation on MOR. Concepts of pore mouth catalysis,[56] a form of partial confinement, have been used as a phenomenological description of processes in which molecules penetrate small zeolite channels only partially as they react. Propane reactions in MOR may well fit this empirical concept, because reactants cannot fully enter the 8-MR pockets within which they preferentially react and remain in part within connecting 12-MR channels (detailed treatments for estimating channel and molecular dimensions shown in Sections S.6 and S.7, respectively, of the Supporting Information). The

(56) Degnan, T. F. *J. Catal.* **2003**, *216*, 32.

Table 6. Monomolecular n-Butane Cracking and Dehydrogenation Rate Constants (k_{meas}) (per total H^+) and Rate Ratios at 748 K Experimentally Measured on MOR-Z Samples and Estimated within 8-MR and 12-MR Locations of MOR

	k_{meas} ($\times 10^3$ mol (mol H^+)$^{-1}$ s^{-1} bar^{-1})			rate ratios	
zeolite	terminal C−C cracking	central C−C cracking	dehyd	terminal/central C−C cracking	cracking/dehyd
$H_{100}Na_0$MOR-Z	13.0	3.2	13.8	4.0	1.1
$H_{83}Na_{17}$MOR-Z	10.2	2.9	12.8	3.5	1.0
$H_{73}Na_{27}$MOR-Z	6.9	2.7	4.9	2.6	2.0
$H_{59}Na_{41}$MOR-Z	6.4	2.4	4.4	2.6	2.0
$H_{45}Na_{55}$MOR-Z	4.0	1.6	2.1	2.6	2.6
8-MR[a]	20.8 ± 5.4	4.1 ± 2.0	31.5 ± 6.0	5.0	0.9
12-MR[a]	n.d.[b]	1.8 ± 1.2	n.d.[b]	n.d.[b]	n.d.[b]

[a] Rate parameters for 8-MR and 12-MR locations determined by least-squares regression. Uncertainties in regressed rate parameters are reported as twice the standard error. [b] n.d., not detected.

Table 7. Measured Activation Energies (E_{meas}) and Entropies (ΔS_{meas}) for Monomolecular n-Butane Cracking and Dehydrogenation on MOR Samples and Estimated Values within 8-MR and 12-MR Locations of MOR

	E_{meas} (kJ mol^{-1})			ΔS_{meas} (J mol^{-1} K^{-1})		
zeolite	terminal C−C cracking[a]	central C−C cracking[a]	dehyd[b]	terminal C−C cracking[c]	central C−C cracking[c]	dehyd[d]
$H_{100}Na_0$MOR-Z	156	153	203	−86	−96	−36
$H_{83}Na_{17}$MOR-Z	160	152	227	−83	−98	−4
$H_{73}Na_{27}$MOR-Z	139	145	213	−114	−108	−31
$H_{59}Na_{41}$MOR-Z	148	146	231	−102	−108	−8
$H_{45}Na_{55}$MOR-Z	145	139	n.d.[f]	−110	−120	n.d.[f]
8-MR[e]	163 ± 15	159 ± 11	215 ± 11	−72 ± 23	−86 ± 19	−13 ± 17
12-MR[e]	n.d.[f]	134 ± 10	n.d.[f]	n.d.[f]	−126 ± 22	n.d.[f]

[a] Errors for experimentally determined cracking E_{meas} are ± 6 kJ mol^{-1}. [b] Errors for experimentally determined dehydrogenation E_{meas} are ± 10 kJ mol^{-1}. [c] Errors for experimentally determined cracking ΔS_{meas} are ± 9 J mol^{-1} K^{-1}. [d] Errors for experimentally determined dehydrogenation ΔS_{meas} are ± 15 J mol^{-1} K^{-1}. [e] Rate parameters for 8-MR and 12-MR locations determined by least-squares regression. Uncertainties in regressed rate parameters are reported as twice the standard error. [f] n.d., not detected.

resulting transition states would preferentially activate terminal C−C and C−H bonds, but such preferences lead to identical products for propane reactants. Any terminal C−C bond activation preference arising from partial confinement would be apparent for n-butane reactants, but specific activation of terminal C−H bonds may be impossible to detect because of fast hydride shifts on both 8-MR and 12-MR acid sites. Indeed, equilibrated n-butene isomers were detected at all conditions on all catalysts (data shown in Section S.8 of the Supporting Information). We use here terminal-to-central C−C bond cleavage rate ratios to probe how molecules access active sites within 8-MR and 12-MR environments and to demonstrate the effects of partial confinement on n-butane dehydrogenation and cracking turnover rates.

Rate constants of terminal and central C−C bond cracking and dehydrogenation of n-C_4H_{10} (per residual H^+) and their rate ratios are shown at 748 K in Table 6 for five MOR samples with varying Na^+ content; the corresponding measured activation energies and entropies are shown in Table 7. Figure 8 shows the temperature dependence of monomolecular rate constants (per residual H^+) for terminal and central C−C bond cleavage (Figure 8a) and of their rate ratio (Figure 8b) on MOR samples with 56% ($H_{100}Na_0$MOR-Z) and 13% ($H_{45}Na_{55}$MOR-Z) of H^+ sites within 8-MR pockets. As Na^+ selectively replaced H^+ within 8-MR locations, terminal and central C−C bond cracking and dehydrogenation rate constants (per total H^+) decreased, while cracking-to-dehydrogenation rate ratios concurrently increased (Table 6, Figure 8). These trends resemble those for propane cracking and dehydrogenation, suggesting that the specificity of OH groups in 8-MR pockets for both reactions, and especially for dehydrogenation, is not restricted to the smaller C_3H_8 reactants. Measured activation energies for terminal and central C−C bond cracking are similar to each other on all samples (Table 7), consistent with the lack of temperature effects on n-C_4H_{10} terminal cracking selectivities on H-MOR (718−778 K; Figure 8b) and of n-C_5H_{12} cracking selectivities on H-MFI (750−810 K).[22] The absence of enthalpic preferences for the cleavage of one of the two types of C−C bonds in n-butane via late carbonium ions as transition states is consistent with the similar gas-phase protolytic cracking enthalpies for the various C−C bonds in n-decane estimated by theory.[57] The terminal-to-central C−C bond cracking selectivity decreased monotonically as H^+ sites within 8-MR pockets were selectively replaced by Na^+ (Table 6), suggesting that terminal bonds are activated preferentially on 8-MR OH sites, as expected from partial confinement of n-butane within these side pockets.

Monomolecular rate constants for H^+ sites within 8-MR and 12-MR locations were estimated from measured rate constants (per H^+) on the five MOR-Z catalysts (using eq 12 and treatments similar to those in Section S.5 of the Supporting Information). These rate constants (733−763 K; shown at 748 K in Table 6) were used to determine activation energies and entropies on acid sites within these two environments (Table 7). As in the case of C_3H_8, n-C_4H_{10} cracking and dehydrogenation rate constants were larger on 8-MR than on 12-MR acid sites. The rates of dehydrogenation and of terminal C−C cracking on 12-MR acid sites were too small to be estimated accurately from overall rate constants, because both reactions occurred much faster on 8-MR acid sites. Measured terminal-to-central cracking rate ratios increased from essentially zero on 12-MR acid sites to 5.0 on sites within 8-MR pockets (Table 6). These data indicate that the partial confinement of n-C_4H_{10} reactants into 8-MR pockets leads to a configurational preference for cracking at terminal C−C bonds in n-butane.

Measured activation energies for central C−C bond cracking of n-C_4H_{10} (Table 7) were higher on sites within 8-MR pockets (159 ± 11 kJ mol^{-1}), where this reaction actually occurs at

(57) Hunter, K. C.; East, A. L. L. *J. Phys. Chem. A* **2002**, *106*, 1346.

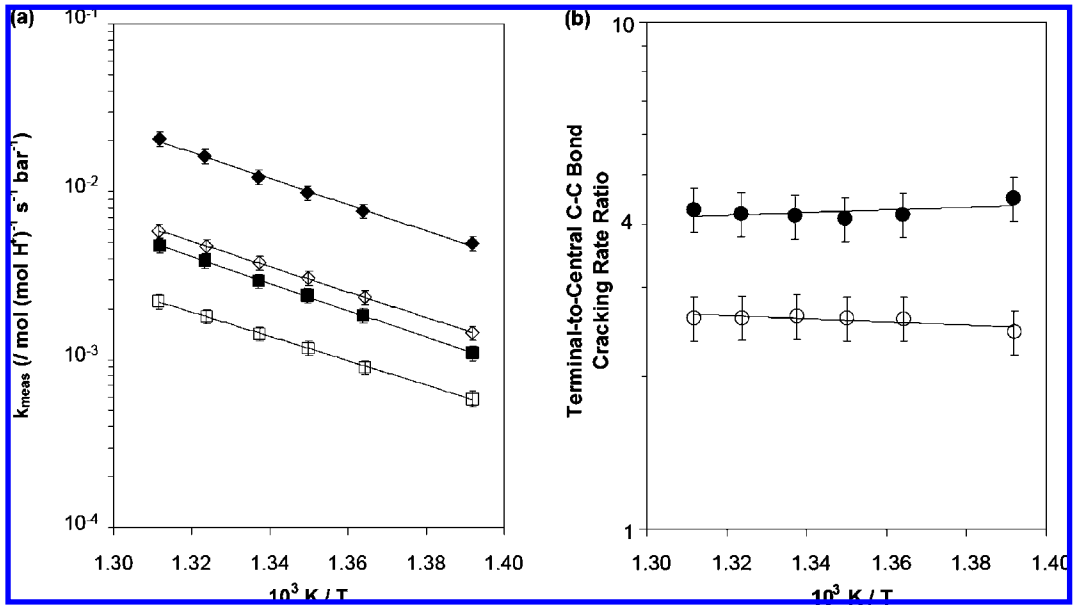

Figure 8. (a) Measured rate constants (k_{meas}) (per total H^+) for terminal C−C bond cracking in n-butane (♦, ◊) and central C−C bond cracking in n-butane (■, □) on H-MOR-Z (closed symbols) and $H_{45}Na_{55}$MOR-Z (open symbols). (b) Dependence of terminal-to-central C−C bond cracking rate ratios of n-butane on temperature on H-MOR-Z (●) and $H_{45}Na_{55}$MOR-Z (○).

higher rates, than in 12-MR channels (134 ± 10 kJ mol^{-1}), as also found for C_3H_8 cracking. Adsorption enthalpies of n-C_4H_{10} in 12-MR channels of H-MOR (−50 kJ mol^{-1})[29] lead to an estimated intrinsic activation barrier for central C−C bond cracking of 184 ± 12 kJ mol^{-1} (using eq 6); this barrier is similar to that reported here for C_3H_8 cracking on 12-MR channels of H-MOR (192 ± 7 kJ mol^{-1}) and in previous studies for cracking of C_3−C_6 n-alkanes on H-MFI (194−198 ± 14 kJ mol^{-1}).[21] If we assume that intrinsic activation barriers for central C−C bond cracking within 8-MR pockets were also similar to these values in 12-MR channels, then we estimate n-butane adsorption energies of −25 kJ mol^{-1} from eq 6, indicating that n-butane binding is weaker than expected from complete confinement within 8-MR pockets (−59 kJ mol^{-1}; Section S.6 of the Supporting Information). These findings indicate that van der Waals interactions stabilize only part of the n-butane molecule (0.83 nm length) and of its terminal cracking transition state within shallow 8-MR pockets (0.37 nm depth). Even for central C−C bond cleavage in n-butane, turnover rates were higher in 8-MR than 12-MR locations, in spite of weaker enthalpic stabilization of cracking transition states in 8-MR pockets, because of concomitantly larger activation entropies (Table 7). These compensating entropic effects appear to reflect the partial protrusion of adsorbed reactants and transition states into connecting 12-MR channels, which decrease the free energy of the transition state, the relevant thermodynamic property that describes its stability. These transition state free energies, referenced to gas-phase reactants, determine measured turnover rates at the conditions of our study (eq 5) and account for the effects of reactant and acid site environment on the rate and selectivity of alkane activation reactions.

Next, we examine whether local spatial constraints also influence reactivity via these entropic effects on transition state stability as the zeolite structure changes. Specifically, we address the role of intrachannel environment on Brønsted acid site reactivity for H-MFI zeolites, for which the structural diversity of T-sites makes Al and OH distributions inaccessible to experiment using existing tools.

Table 8. Monomolecular Propane Cracking and Dehydrogenation Rate Constants (k_{meas}) and Cracking-to-Dehydrogenation (C/D) Rate Ratios Measured at 748 K on Different H-MFI Samples and Measured Activation Energies (E_{meas})

	k_{meas} (× 10^3 mol (mol H$^+$)$^{-1}$ s^{-1} bar^{-1})			E_{meas} (kJ mol^{-1})	
zeolite	cracking	dehyd	C/D ratio	cracking[a]	dehyd[b]
H-MFI-1	2.0	2.1	0.9	158	200
H-MFI-2	6.3	3.9	1.6	155	204
$H_{85}Na_{15}$MFI-2	3.9	1.5	2.7	150	193
H-MFI-3	4.4	3.5	1.3	150	200
H-MFI-4	1.5	0.8	1.9	150	194

[a] Errors are ± 5 kJ mol^{-1}. [b] Errors are ± 7 kJ mol^{-1}.

3.4. Monomolecular Propane Activation on H-MFI Zeolites. Rate constants for propane cracking and dehydrogenation (per H^+) and cracking-to-dehydrogenation rate ratios at 748 K, and measured cracking and dehydrogenation activation energies are shown in Table 8 on H-MFI samples of different provenance and acid site density. Measured activation barriers were 40−50 kJ mol^{-1} higher for dehydrogenation than for cracking, as also found for H-MOR. Consequently, cracking-to-dehydrogenation rate ratios decreased with increasing temperature on all H-MFI samples. Cracking and dehydrogenation turnover rates (per H^+) varied among these H-MFI samples (by up to factors of 5), without any systematic trends with their Al content. These turnover rates (or their ratios) did not correlate with the concentration of extraframework Al atoms or Lewis acid centers, as shown by the NMR and IR data in Sections S.1 and S.2, respectively, of the Supporting Information.

These turnover rate differences (Table 8) suggest that Brønsted acid sites at the 12 T-sites in MFI are not identical in reactivity and that these samples differ in their distribution of Al among these locations. In contrast, earlier studies reported n-hexane cracking activities that did not depend on Al content[1,2,33] and inferred that the location of the sites were also inconsequential for reactivity. These data would also be consistent with location-specific reactivity but for a set of samples in which Al

is similarly distributed among T-sites for all Al contents, a possibility mentioned in the original article,[33] but largely ignored thereafter. In spite of similar acid strength, the reactivity of Brønsted acid sites in MFI depends on location, as shown here for H-MOR (Section 3.2) and appears to account for the turnover rate differences among our H-MFI samples (Table 8). We conclude that previous studies in which n-hexane cracking rates were independent of Al content[1,2,33] may have used H-MFI samples with a similar distribution of acid sites among locations of different reactivity. We cannot comment further about these discrepancies or about the extent to which bimolecular pathways prevailed during these previous studies, because precise experimental conditions were not given and the cracking data were reported as catalytic activities (arbitrary units) that were likely measured under integral reactor conditions.

The replacement of just 15% of H^+ sites in H-MFI-2 by Na^+ decreased C_3H_8 cracking and dehydrogenation turnover rates (per H^+) (by ~1.5 and ~2.5 factors, respectively) and increased their selectivity ratios (from 1.6 to 2.7) (Table 8), but measured activation energies for neither cracking nor dehydrogenation were affected. These effects of Na^+ exchange on monomolecular C_3H_8 cracking and dehydrogenation turnover rates (per H^+) on H-MFI resemble those attributed here in the case of H-MOR to the preferential replacement of H^+ by Na^+ at locations where cracking and dehydrogenation catalysis is most effective (Table 4). These effects of alkali exchange are also similar to those reported for i-C_4H_{10}[58] and n-C_6H_{14}[59] cracking on H-USY, in which cracking rates were rendered undetectable upon titration of just 20−33% of the H^+ species associated with framework Al atoms. Our data show that Na^+ cations preferentially replace Brønsted acid sites with the highest reactivity for reactions involving cationic transition states. We conclude also that electropositive Na^+ cations preferentially reside within smaller channel environments, where entropy-enthalpy trade-offs resulting from partial confinement are most consequential. In MFI, however, the structural diversity of T-site locations precludes rigorous assessment of Al siting and prevents unequivocal and specific interpretations of the effects of local environment on cracking and dehydrogenation of alkanes.

The preferential reactivity of specific channel environments reported here for alkane activation on Brønsted acid sites and earlier for CO insertion into surface methyls[8] appear to represent general features of catalytic reactions involving cationic transition states. Spatial constraints imposed by zeolite channels, frequently proposed to select transition states based simply on their size and shape, play a more fundamental and consequential role in acid catalysis via solvation of cationic transition states and specifically via its mediation of enthalpy and entropy factors, predominantly in ways that favor entropic stabilization even at the expense of enthalpic penalties. We expect that similar effects will prevail for bimolecular alkane reaction pathways that propagate via hydride transfer and β-scission and oligomerization cycles, channel environments permitting the formation of the bulkier transition states involved, because these pathways also require the formation of cationic transition states.[6,7] Our findings about the dominant role of entropy and of partial containment provide a conceptual path forward toward a more rigorous assessment of local environment effects on transition state stability and therefore on site reactivity and selectivity and toward more rational design and selection strategies for microporous catalysts with specific catalytic properties.

4. Conclusions

Turnover rate (per H^+) differences for monomolecular cracking and dehydrogenation of propane and n-butane with changes in zeolite structure (H-MFI, H-FER, and H-MOR) and acid site location (H-MOR: 8-MR side pocket, 12-MR main channel) reflect the strong dependence of cationic transition state free energy on local channel environment. In agreement with Born−Haber thermochemical cycles that define energy relations in acid catalysis, intrinsic activation barriers for both monomolecular propane cracking (201−208 kJ mol^{-1}) and dehydrogenation (229−245 kJ mol^{-1}) were similar on H-MFI, H-FER, and H-MOR samples and were consistently larger for dehydrogenation (by 25−42 kJ mol^{-1}). The insensitivity of these barriers to zeolite structure reflects similar zeolite deprotonation enthalpies and commensurate differences in the stabilization of transition states and reactants by different channel environments. Transition states for dehydrogenation are higher in energy than for cracking, reflecting respective affinities for protonation at C−C and C−H bonds in gas-phase alkanes, and are higher in entropy than for cracking, consistent with the later and looser transition states for the former pathways as suggested by theory.

Monomolecular cracking and dehydrogenation reactions of propane and n-butane occurred predominantly on Brønsted acid sites located within 8-MR side pockets of H-MOR, a consequence of spatially constrained environments that allow only partial containment of reactants and transition states. Partial transition state confinement results in entropy gains that compensate for concomitant enthalpy losses and decrease transition state free energies. Such strong effects of channel environment and, by extension, acid site location on reactivity allowed for systematic and precise control of cracking-to-dehydrogenation selectivities and of terminal-to-central C−C bond cleavage selectivities by selective titration of OH groups in 8-MR pockets of MOR with Na^+.

These findings reflect the broad range of reactivities likely to prevail among acid sites located within different channels of the same zeolite structure, shown explicitly for MOR samples of varying provenance and acid site distribution and consistent with data obtained on different MFI samples. In what appears to be a consideration specific to and consequential for acid catalysis by zeolite, channel environments influence the formation of cationic transition states, more fundamentally than simple considerations of size and shape, through their solvation of transition states and mediation of compromises in enthalpy and entropy factors. These findings and their conceptual interpretations offer specific design and selection strategies for microporous solids of specific channel structure and acid site location with predictable consequences for acid catalysis.

Acknowledgment. The authors thank Dr. Stacey I. Zones (Chevron) for the MFI samples. We thank Dr. Zones along with Prof. Aditya Bhan (University of Minnesota at Twin Cities), Josef Macht (University of California at Berkeley), and Prof. Johannes A. Lercher (Technische Universität München) for helpful discussions. We also thank Dr. Sonjong Hwang (California Institute of Technology) and Dr. Chul Kim (California Institute of Technology) for collecting the ^{27}Al NMR spectra reported here. Finally, we acknowledge with thanks the financial support from Chevron Energy Technology Company.

(58) Beyerlein, R. A.; McVicker, G. B.; Yacullo, L. N.; Ziemiak, J. J. *Abstr. Pap.—Am. Chem. Soc.* **1986**, *191*, 7-PETR.
(59) Fritz, P. O.; Lunsford, J. H. *J. Catal.* **1989**, *118*, 85.

Supporting Information Available: Experimental methods and ^{27}Al NMR spectra for zeolite samples; experimental methods and IR spectra for zeolite samples upon adsorption of CO at 123 K; assessment of transport corruptions using Mears criteria; detailed derivations of rate laws and activity coefficients using transition state treatments for thermodynamically nonideal systems; description of least-squares regression methods used for rate constant estimation in 8-MR and 12-MR locations of MOR; estimation of adsorption parameters in 8-MR pockets of MOR; estimation of 8-MR MOR pocket depth and kinetic diameters of molecules; kinetic data for butene isomer distributions on MOR samples. This material is available free of charge via the Internet at http://pubs.acs.org.

JA808292C